



Fermi National Accelerator Laboratory

FERMILAB-TM-1730

Antiproton Production for Tevatron

I. L. Azhgirey, N. V. Mokhov, S. I. Striganov

*Institute for High Energy Physics
Protvino, USSR*

March 1991



Operated by Universities Research Association Inc. under contract with the United States Department of Energy

ANTIPROTON PRODUCTION FOR TEVATRON

I.L.Azhgirey, N.V.Mokhov, S.I.Striganov

Institute for High Energy Physics, Protvino, USSR

June 19, 1990

Needs to improve the Fermilab Pbar Source for the Tevatron Upgrade and discrepancies [1,2] in predictions of the antiproton yields have forced us to develop the production model based on the modern data and to incorporate this model to the current version of MARS10 code [3]. The inclusive scheme of this code with the use of statistical weights allows the production of antiprotons to be enhanced within the phase -space region of interest, which is extremely effective for optimization of Pbar Source parameters and for developing of such an idea as a beam sweeping system [4].

Antiproton production model included in the modified version of our Monte Carlo program MARS10M for the inclusive simulation of hadronic cascades, as for other particles throughout the program, is based on a factorization approach for hadron-nucleus differential cross-section, described in [5-8]. To describe antiproton inclusive spectra in pp-collisions a phenomenological model [9] has been used modified in the low-Pt region ($P_t < 0.2 \text{ GeV}/c$). The antiproton production in pion-nucleon interactions is described in the frame of our simple phenomenological model based on the modern data [8]. In describing of the antiproton production cross-sections ratio in hadron-nucleus and hadron-nucleon collisions the ideas of soft hadronization of color strings [10] and all the present experimental data have been used [8].

Some comparisons of our model with experimental data are presented in Figs.1-7 in the wide intervals of initial momenta, antiproton kinematical variables and nuclei. In all the cases the agreement is pretty good what gives us an assurance in the consequent studies carried out for the Fermilab Pbar Source. The results of such study are presented below.

The following standard Fermilab parameters have been used: proton energy 120 GeV, antiproton momentum $8.9 \text{ GeV}/c$, longitudinal momentum acceptance $\pm 2\%$, target length 7 cm for copper and 5 cm for tungsten, Li lens length 15 cm, Li lens distance to focal plane 14.45 cm, Li lens radius 1 cm (mostly). Other parameters - acceptance and beam spot size - were subject to study for both targets and additionally for the CERN case iridium target. In all cases

$\sigma = \sigma_{max} = \sigma_{may}$ - R.M.S. beam spot size in mm,

$A = Ax = Ay$ -- acceptance of Pbar Source in $\pi \text{ mm mrad}$.

Fig.8 shows antiproton momentum spectra in 120 GeV proton-tungsten collision integrated over two angular intervals as predicted by our model, by phenomenological model [11], which was the base for the Pbar Design Report, and by the multi-chain fragmentation model [12]. The disagreement of factor of 2 or 3 was mentioned first in [1,2]. This difference results in overestimation of antiproton yields in the Design Report (see again [1,2]): Fig.9 confirms this for tungsten target.

Antiproton yield of copper target is shown in Fig.10 for three beam sizes. Having a strong dependence on the last one at small acceptances, yield is the only weak function of σ at the large A . At $A = 20 \pi \text{ mm mrad}$ pbar yield of tungsten target is about 30% higher compare to the copper one. Fig.11 shows the dependence of yield on the maximum angular divergence of antiprotons downstream of the

copper and tungsten targets. As in [13] the graph was produced by fixing the value of theta and varying the maximum displacement of the constant area ellipse until a maximum yield was obtained. For two acceptances shown the yield grows fastly up to $\theta=30$ mrad and is constant after $\theta=45$ mrad which exactly corresponds to the lens parameters ($R=1$ cm etc.). Therefore all other data in this paper are presented for $\theta=45$ mrad. Following [13] the maximum antiproton yield into the Source is obtained by matching the machine acceptance through the injection line and collector lens to an ellipse at the end of the target which contains the maximum number of pbars.

The antiproton yield versus the proton beam spot size is presented in Figs.12-13 for both targets and for various acceptances. Note rather weak dependence in the considered range of sigmas. Calculated fraction of antiprotons originating from secondary interactions in copper and tungsten targets is shown to be a growing function of an acceptance (Fig.14).

As has been shown in [2] the maximum energy deposition E_m in typical targets for antiproton production scales as

$$E_m \text{ (GeV/g)} = C/\sigma^{**n},$$

where σ is R.M.S. beam spot size in mm, C and n are energy- and material-dependent parameters. Correspondingly, the tolerable number of protons in the fast beam pulse on target can be determined as

$$N_p \text{ (ppp)} = \frac{Q * 10^{**10}}{1.6 * E_m} = B * \sigma^{**n},$$

where Q in J/g is melting or shock wave limit for the target material.

Calculating with current version of MARS10M energy deposition distributions in targets one can get the data presented in Figs. 15-16. Resulting parameters of the correspondent fits for the Fermilab Pbar Source proton momentum $p_0 = 120$ GeV/c are given in Table 1 for three targets.

Table 1. Fit parameters.

Target material	Cu	W	Ir (*)
Length (mm)	70.	50.	55.
Diameter (mm)	10.	10.	3.
C	.135	.625	.70
n	1.35	1.0	1.0
Q (J/g)	460	200	360
$B, 10^{**12}$	21.3	2.0	3.2

*) CERN sort of target, surrounded by graphite.

Table 2 collects the calculated data for various targets on the antiproton yield for 20 pi mm mrad acceptance, maximum tolerable numbers of protons on the targets and resulting number of antiprotons in the 1 cm radius Li-lens for such a spill. The corresponding maximum number of antiprotons collected per second is presented in Fig.17. One can see how preferable is copper target for the Fermilab case. Another important conclusion - the increasing with the beam size antiproton rate - is resulted from very different dependences on the beam size: weak for the yield (Figs.12-13) and very strong for the maximum energy deposition (Fig.15). There is no indication on the possible profit of the beam sweeping system for the Pbar Source parameters.

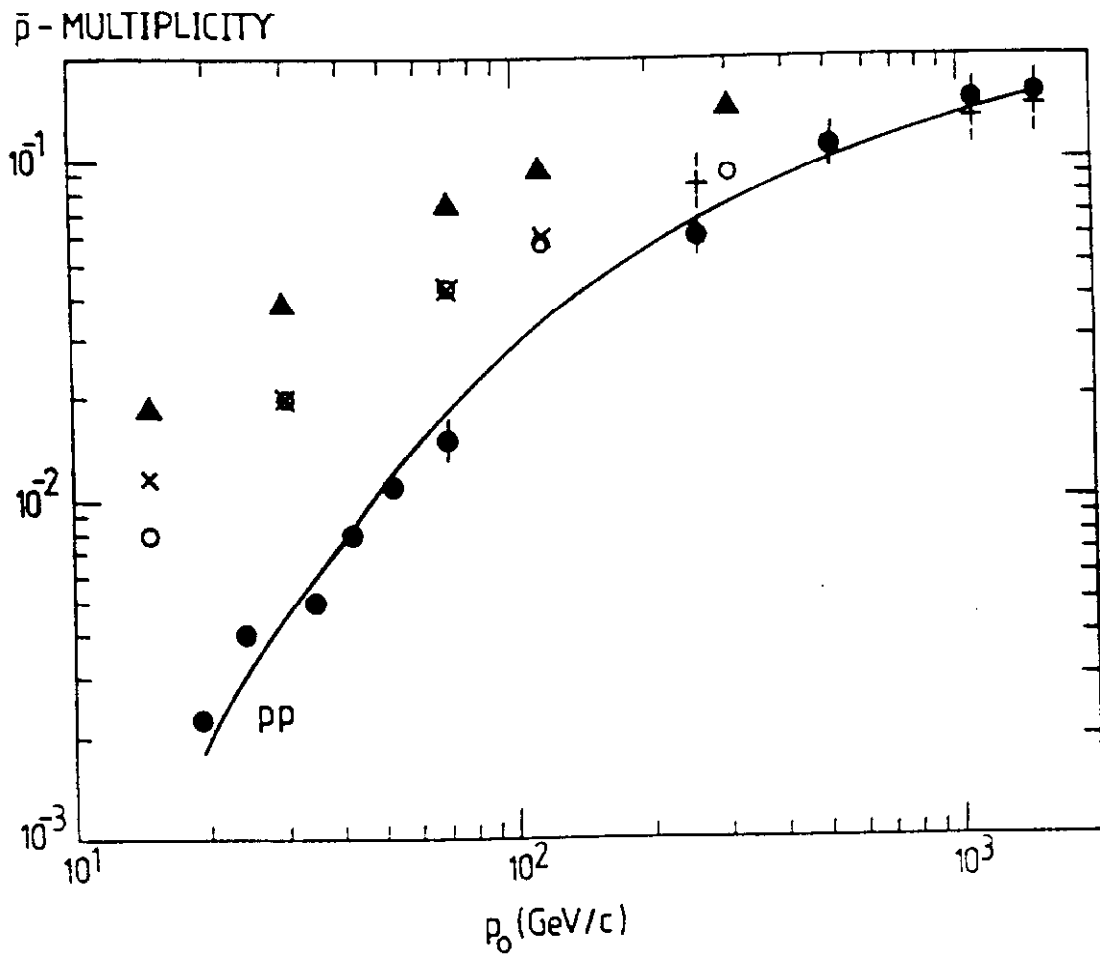
Taking into account the CERN's numbers for antiproton loss in the lens, in titanium windows, beam-gas scattering in injection line etc. one should multiply the data of Fig.17 by factor ~ 0.6 to get the real antiproton collection rate in the Fermilab Pbar Source.

Table 2. Pbar yield, max. proton beam intensity and pbar coilection rate for 20 pi mm mrad acceptance.

Value	Target	R.M.S. beam spot size, sigmax=sigmay (mm)				
		0.05	0.10	0.22	0.30	0.38
Yield, (10E-5 p/proton)	Cu	2.97	2.87	2.57	2.18	1.94
	W	4.14	3.90	3.40	2.89	2.50
	Ir	4.35	4.33	3.80	3.25	2.84
Max. no. of protons, (10E12 PPP)	Cu	0.37	0.95	2.76	4.19	5.77
	W	0.10	0.20	0.44	0.60	0.76
	Ir	0.16	0.32	0.71	0.96	1.22
Pbars collected, (10E7 pbars/pulse)	Cu	1.10	2.73	7.09	9.13	11.2
	W	0.41	0.78	1.50	1.73	1.90
	Ir	0.70	1.38	2.70	3.12	3.46

REFERENCES

1. G. Dugan. Pbar Note-474, Fermilab (1988).
2. I.L. Azhgirey and N.V. Mokhov. Fermilab TM-1529 (1988).
3. N.V. Mokhov. Fermilab FN-509 (1989).
4. C.M. Bhat and N.V. Mokhov. Fermilab TM-1585 (1989).
5. A.N. Kalinovsky, N.V. Mokhov and Yu.P. Nikitin. Passage of High Energy Particles through Matter, AIP, (1989).
6. N.V. Mokhov, S.I.Striganov and A.V. Uzunian. Preprint IHEP 87-59, Serpukhov (1987).
7. N.V. Mokhov. Sov. J. Part. Nucl. v. 18, pp.408-426 (1987).
8. I.L. Azhgirey, N.V. Mokhov and S.I. Striganov. (In preparation).
9. L.C. Tang and L.K. Ng. J. Phys. G.: Nucl. Phys. v. 9, p. 1289 (1983).
10. B.Z. Kopeliovich and F. Niedermayer. Phys. Letters, v. B151, p. 437 (1984).
11. C. Hojvat and A. Van Ginneken. Nucl.Instr.Methods, v.206, p.67(1983).
12. P.A. Aarnio, A. Fasso, H.J. Mohring et al. CERN TIS-RP/168 (1986).
13. N. Walker. CERN/PS/88.69 (AR) (1988)..

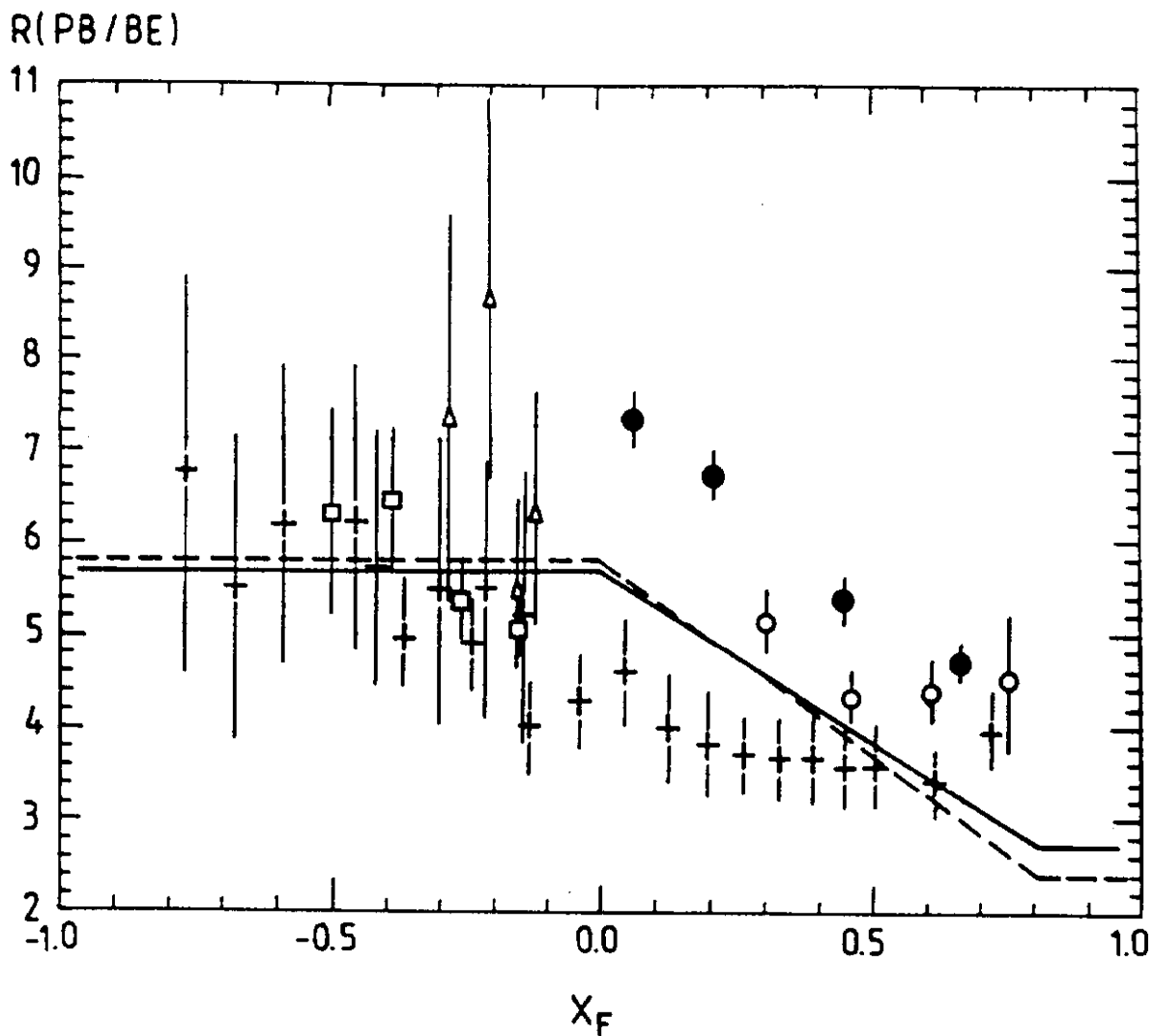


$pp \rightarrow \bar{p} X :$

$+$, \bullet - Experiment
 --- - MARS10

$\pi p \rightarrow \bar{p} X :$

\times - $\pi^+ p$, FLUXA86
 \circ - $\pi^+ p$ } MARS10
 \blacktriangle - $\pi^- p$ }

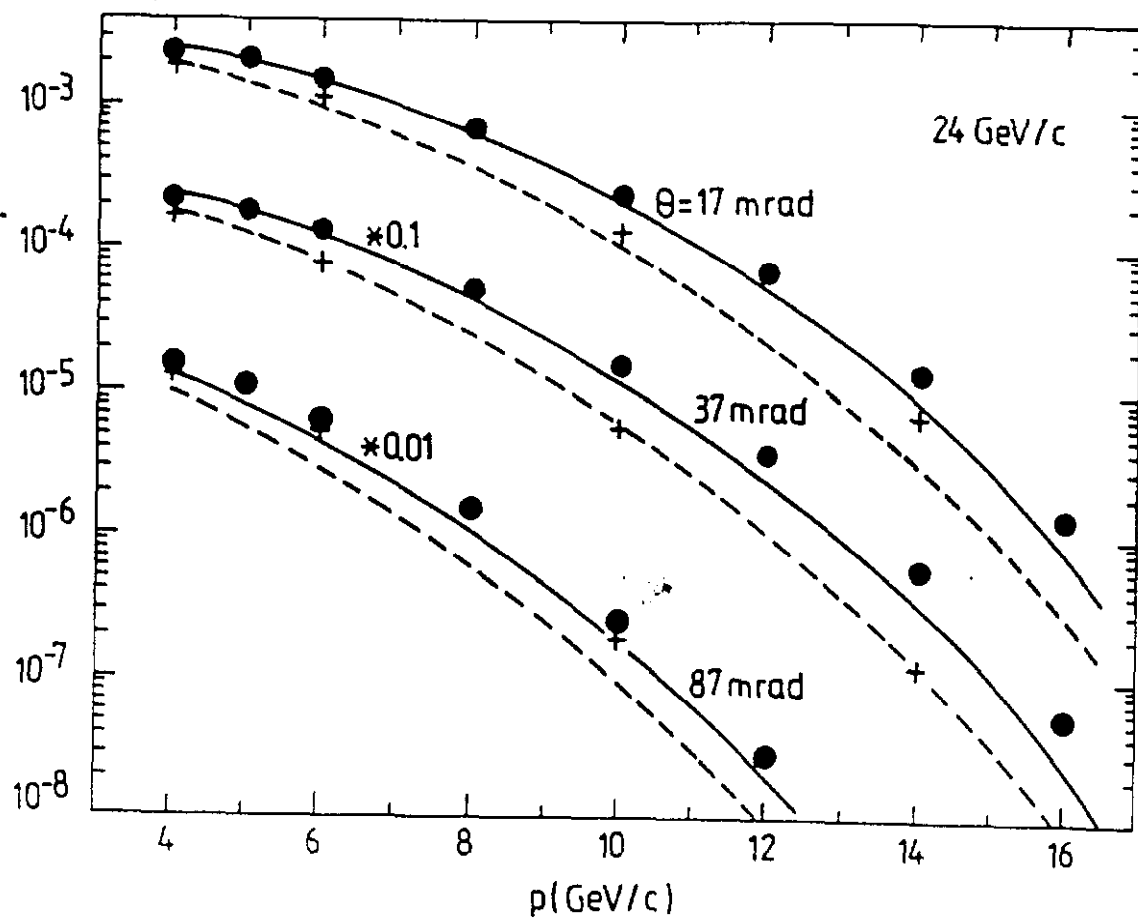


$$R = \frac{\Sigma \frac{d^3\sigma}{dp^3} (pPb \rightarrow \bar{p}X)}{\Sigma \frac{d^3\sigma}{dp^3} (pBe \rightarrow \bar{p}X)}$$

Symbols - experimental data at $p_T = 0, 0.2, 0.5 \frac{\text{GeV}}{c}$
 $p_0 = 12 - 400 \frac{\text{GeV}}{c}$

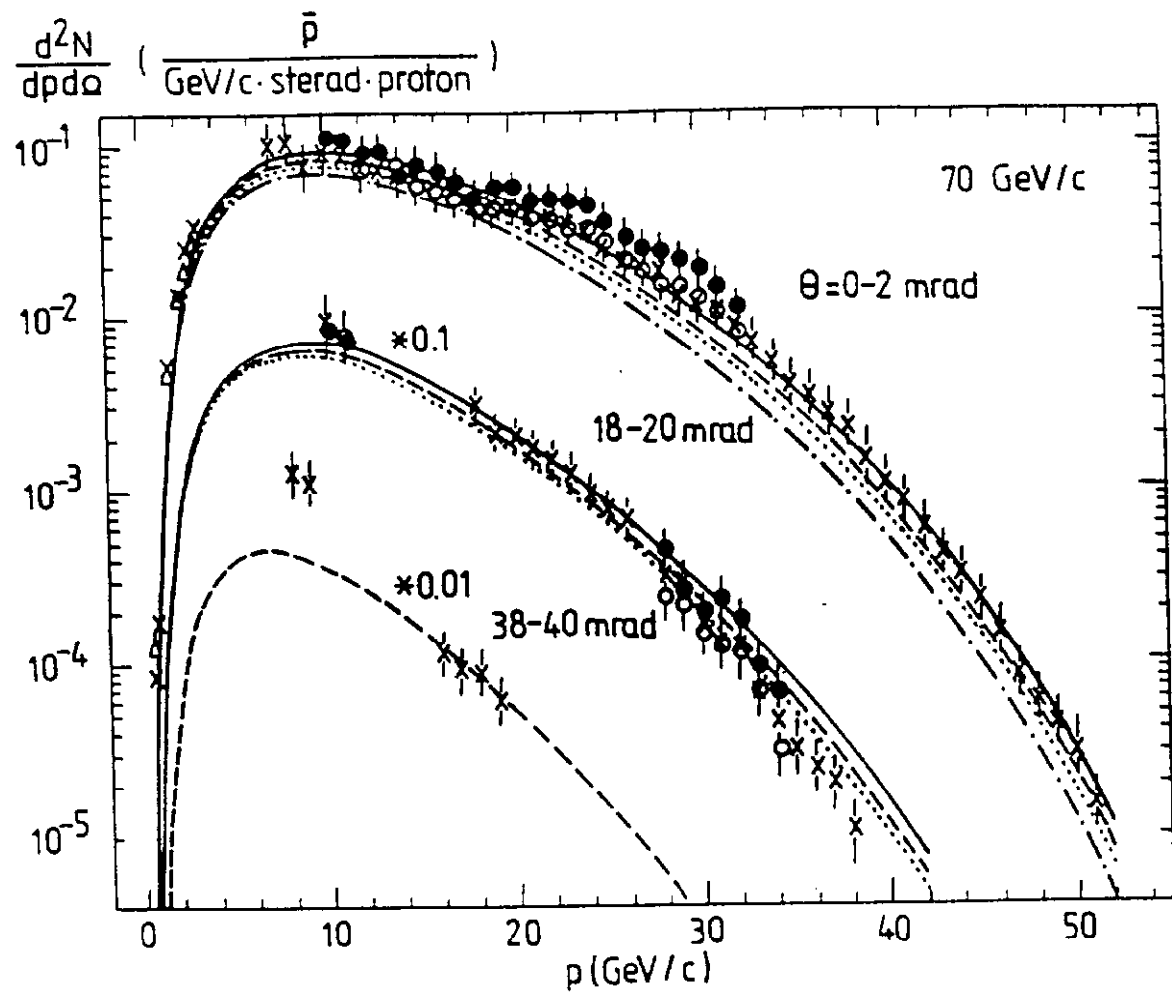
— 70 GeV/c } MARS10
 --- 10 GeV/c }

$E d^3N / d p^3 (\text{GeV}^2 c^3)$



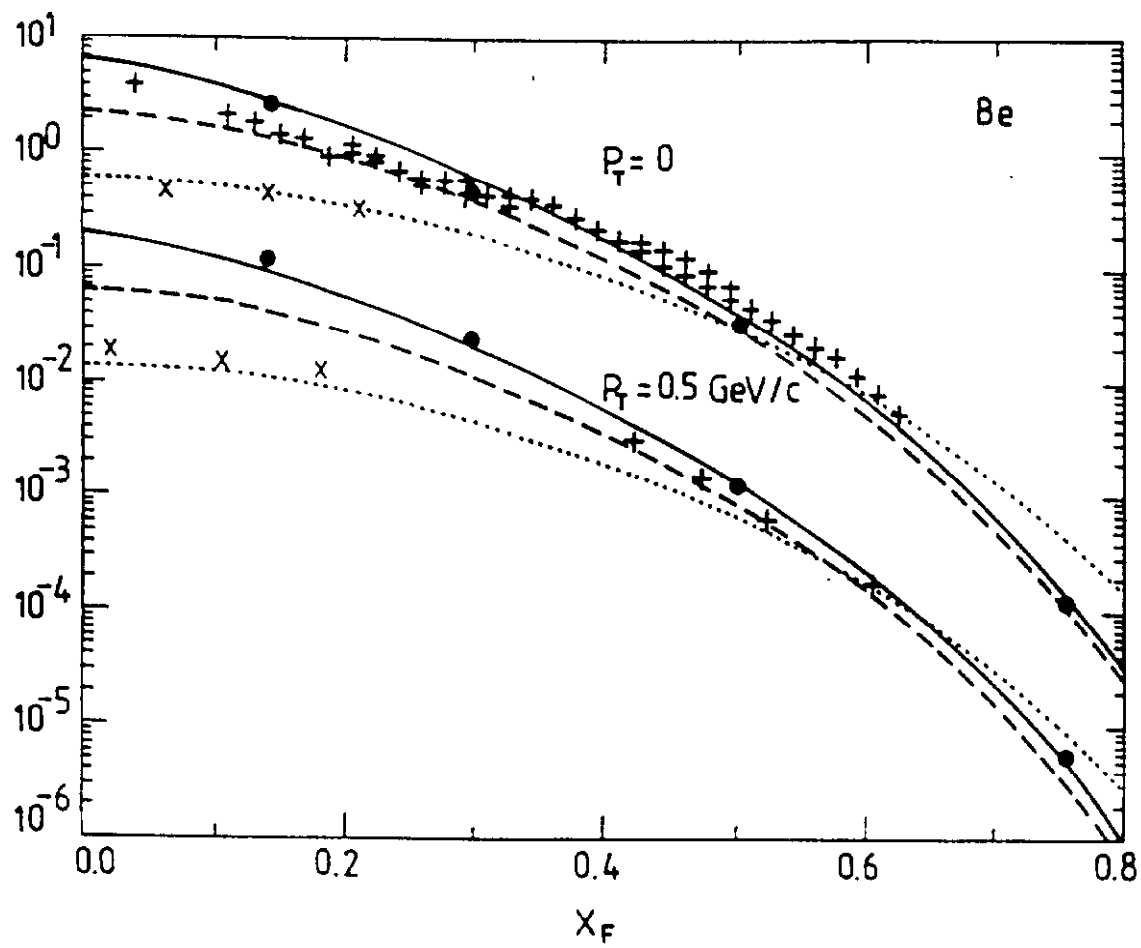
$\bullet \quad \text{Be}$ $+$ Pb

Symbols experiment
Curves - MARS10



Be
 Al
 Cu
 W

$$E d^3G / dp^3 (\text{mb} \cdot \text{GeV}^2 c^3)$$

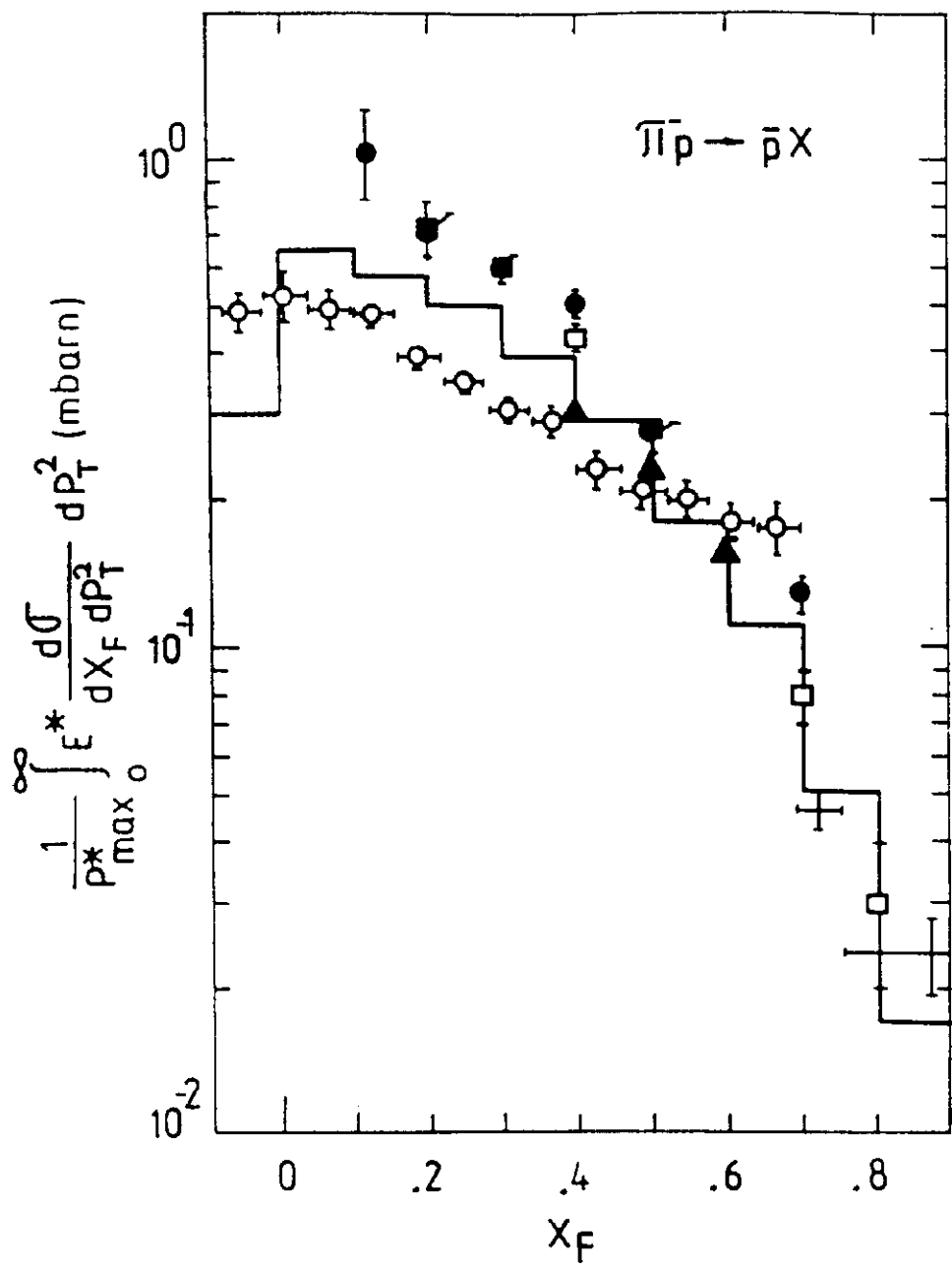


symbols - experiment
Curves - MARS10

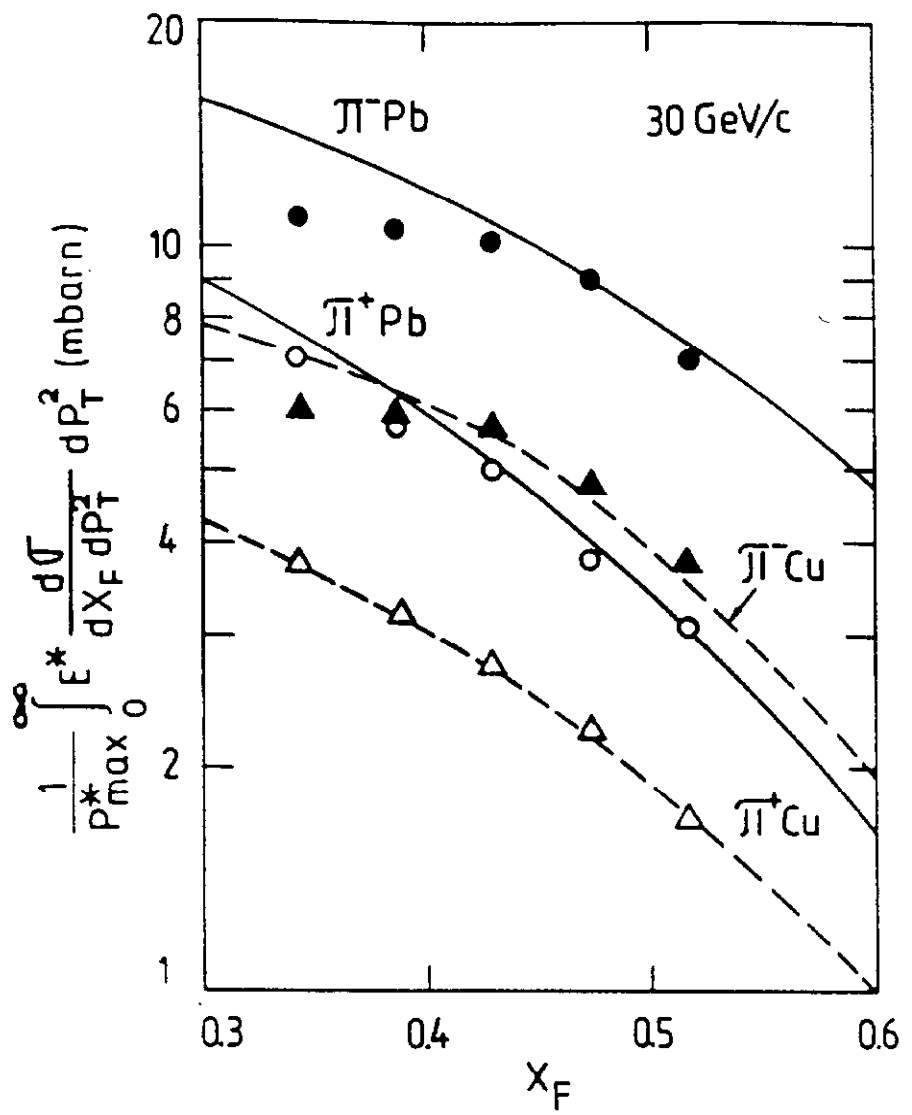
... } - 24 GeV/c

- - - } - 67 GeV/c

- - - } - 400 GeV/c

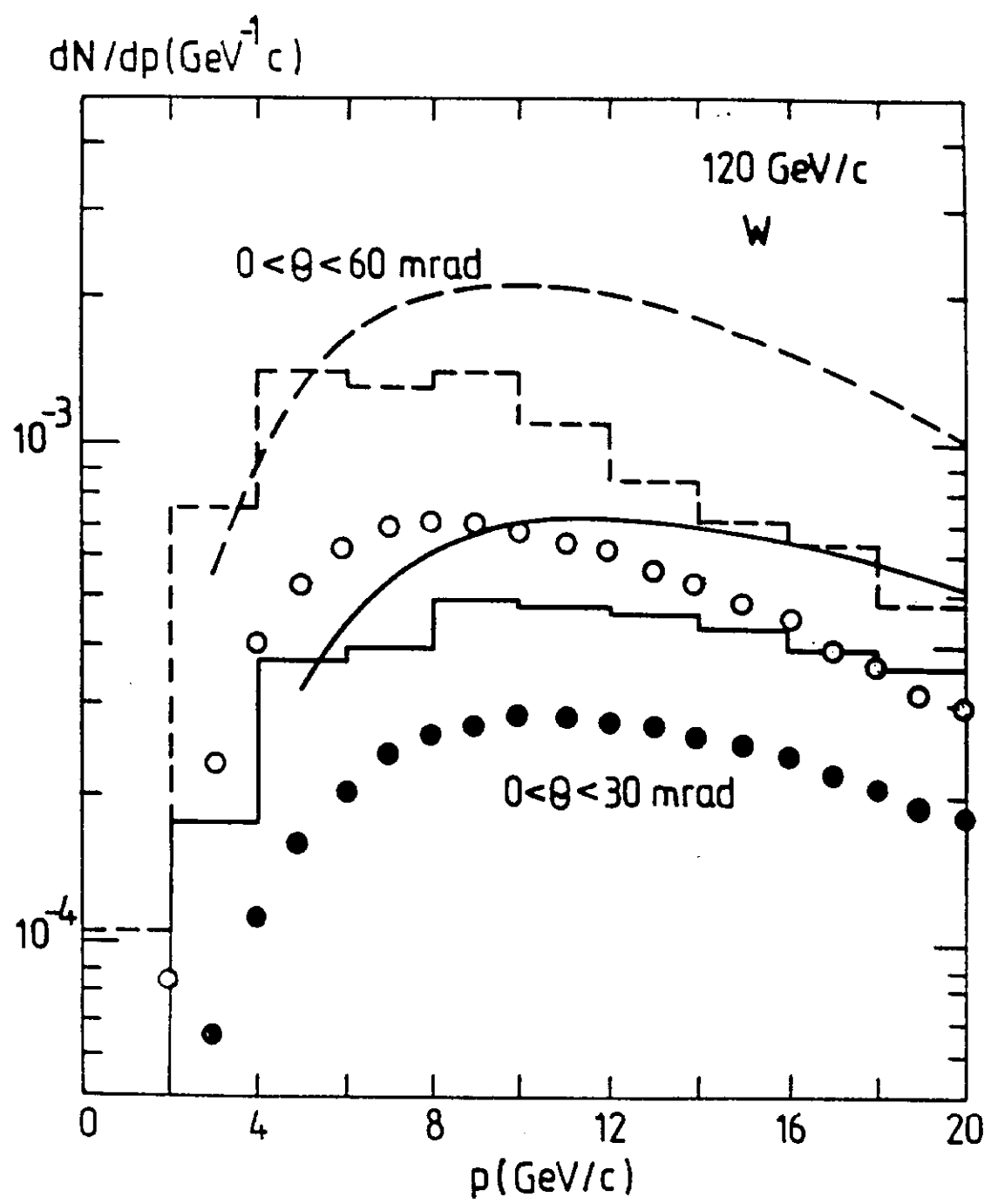


symbols - experiment, 30 and 270 GeV/c
 Histogram - MARS10 , 100 GeV/c



Symbols - experiment

Curves - MARS10



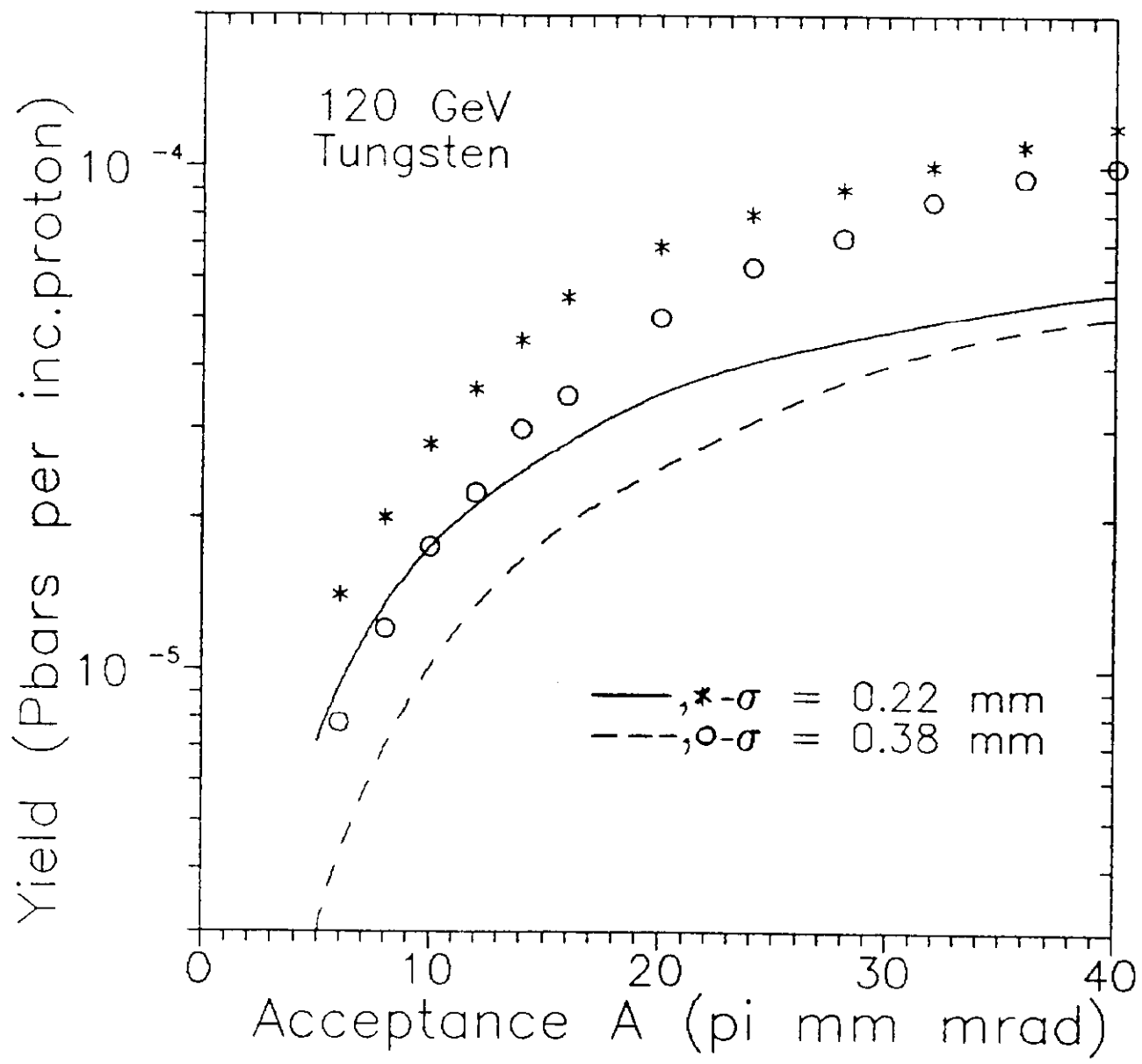
Curves - \bar{p} Design Report (Van Ginneken, Hojvat)

Histograms - FLUKA86

Symbols - MARS10

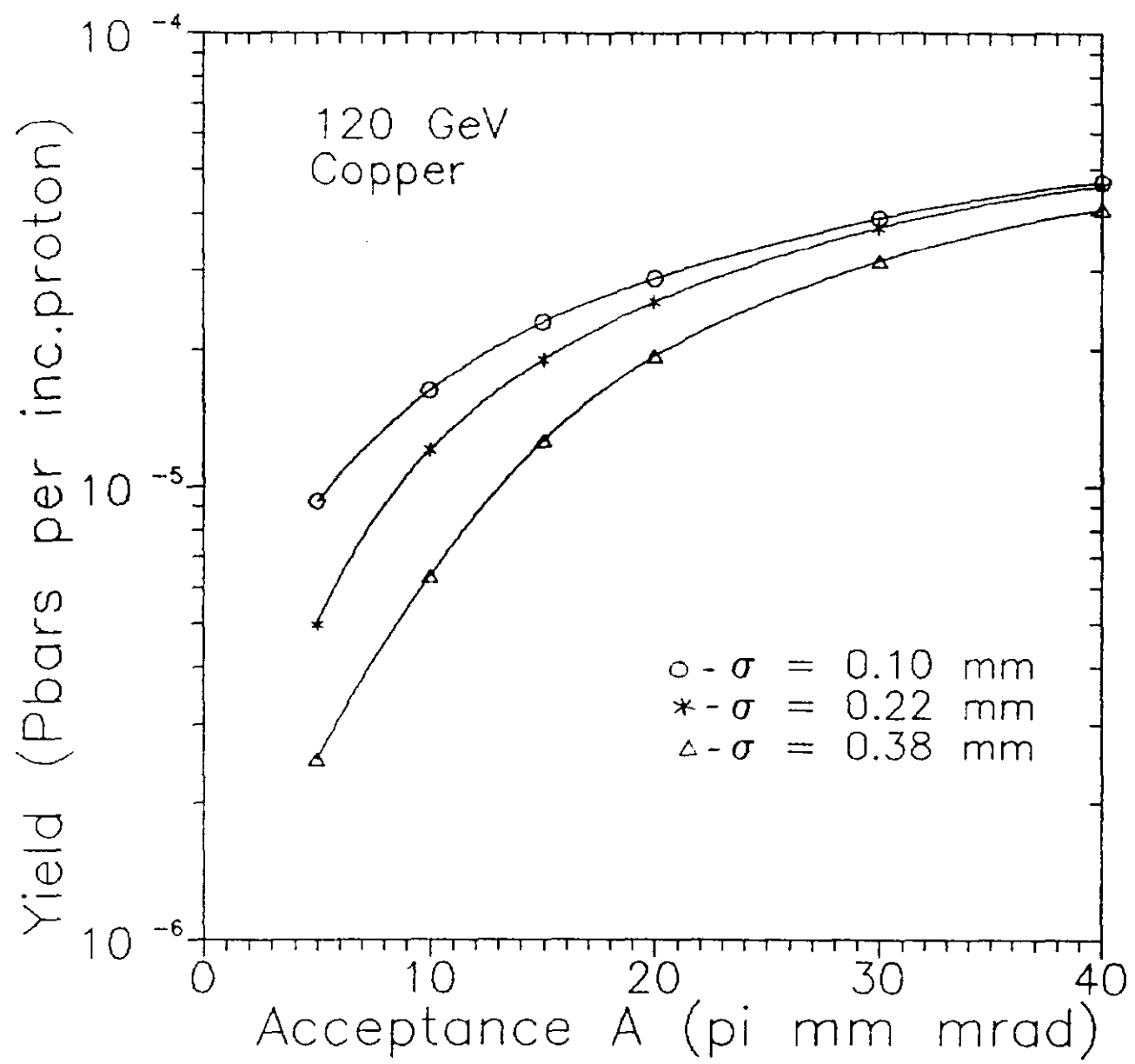
$\frac{\text{---}}{\text{---}} \left\{ \begin{array}{l} \theta < 60 \text{ mrad} \\ \text{---} \end{array} \right.$

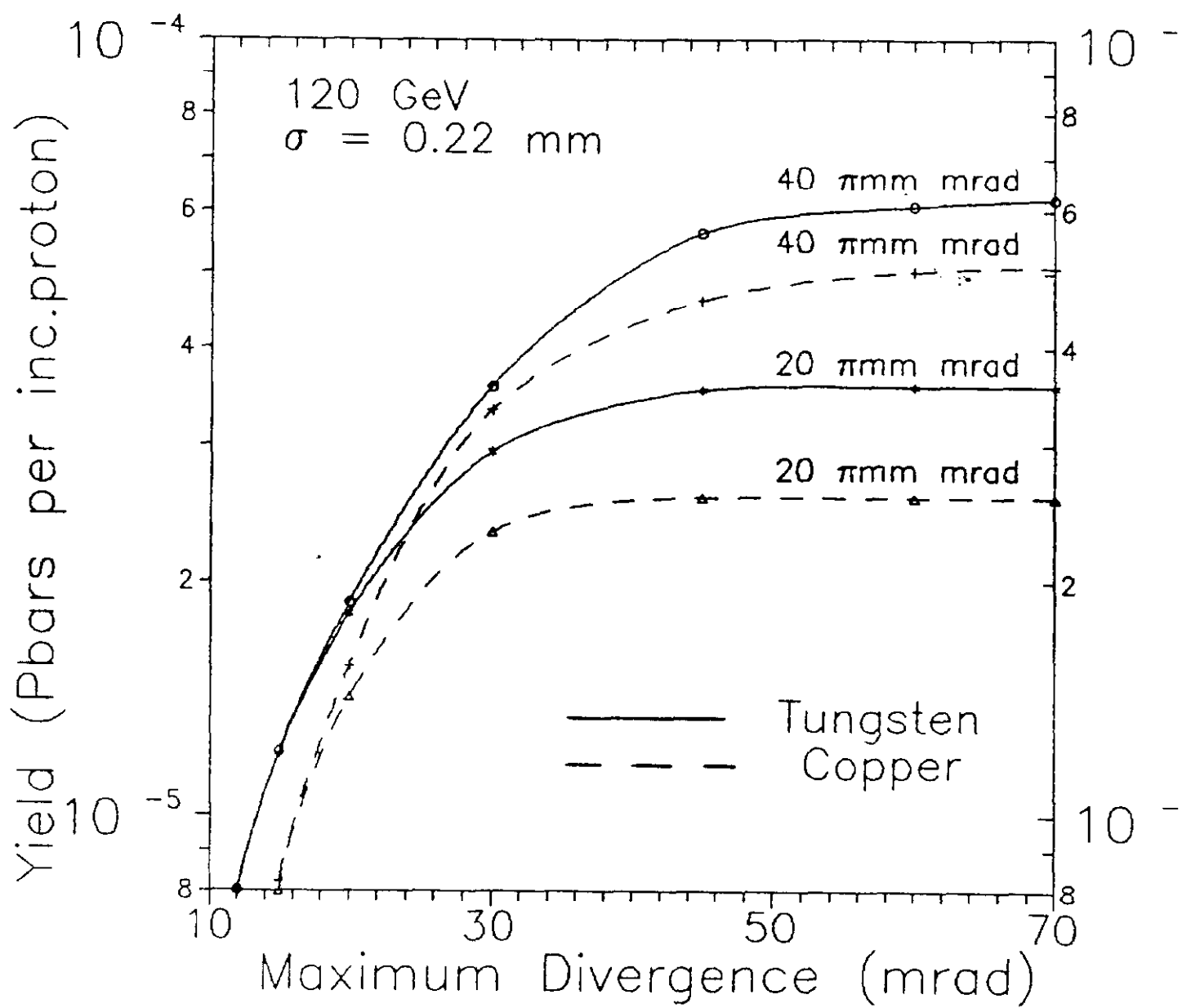
$\frac{\text{---}}{\text{---}} \left\{ \begin{array}{l} \theta < 30 \text{ mrad} \\ \text{---} \end{array} \right.$

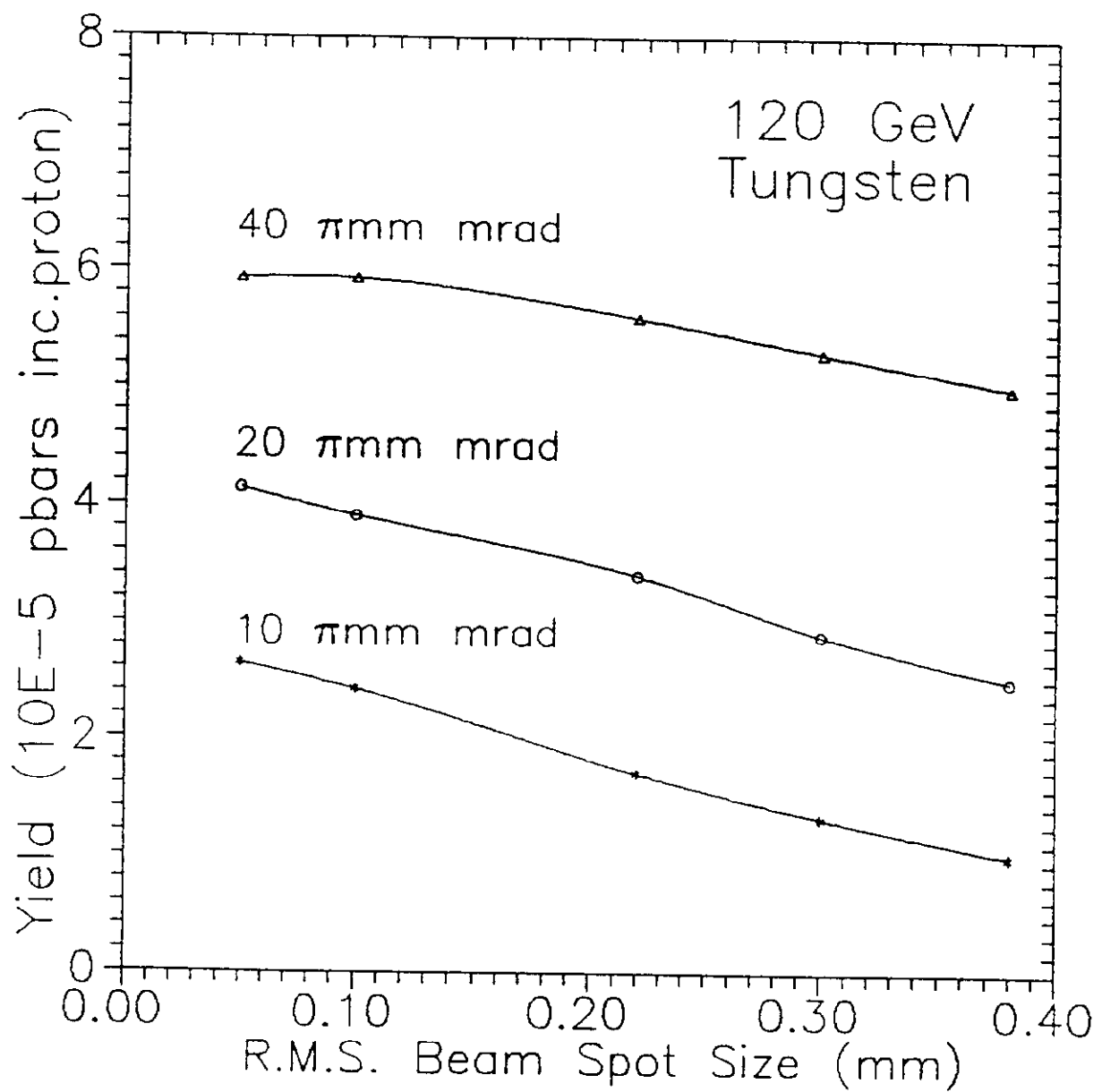


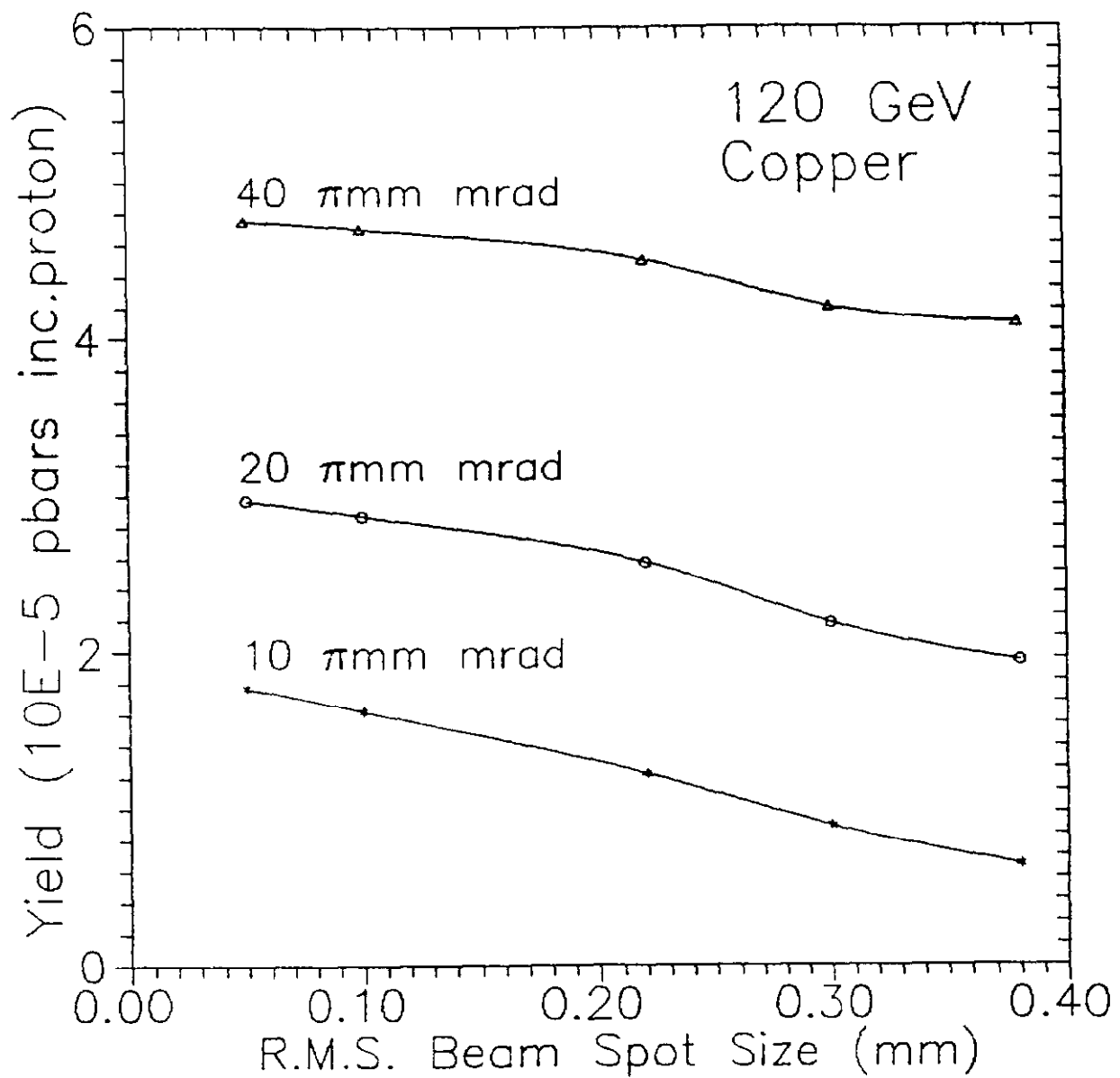
symbols - \bar{p} Design Report (Hojvat, Vercimak)

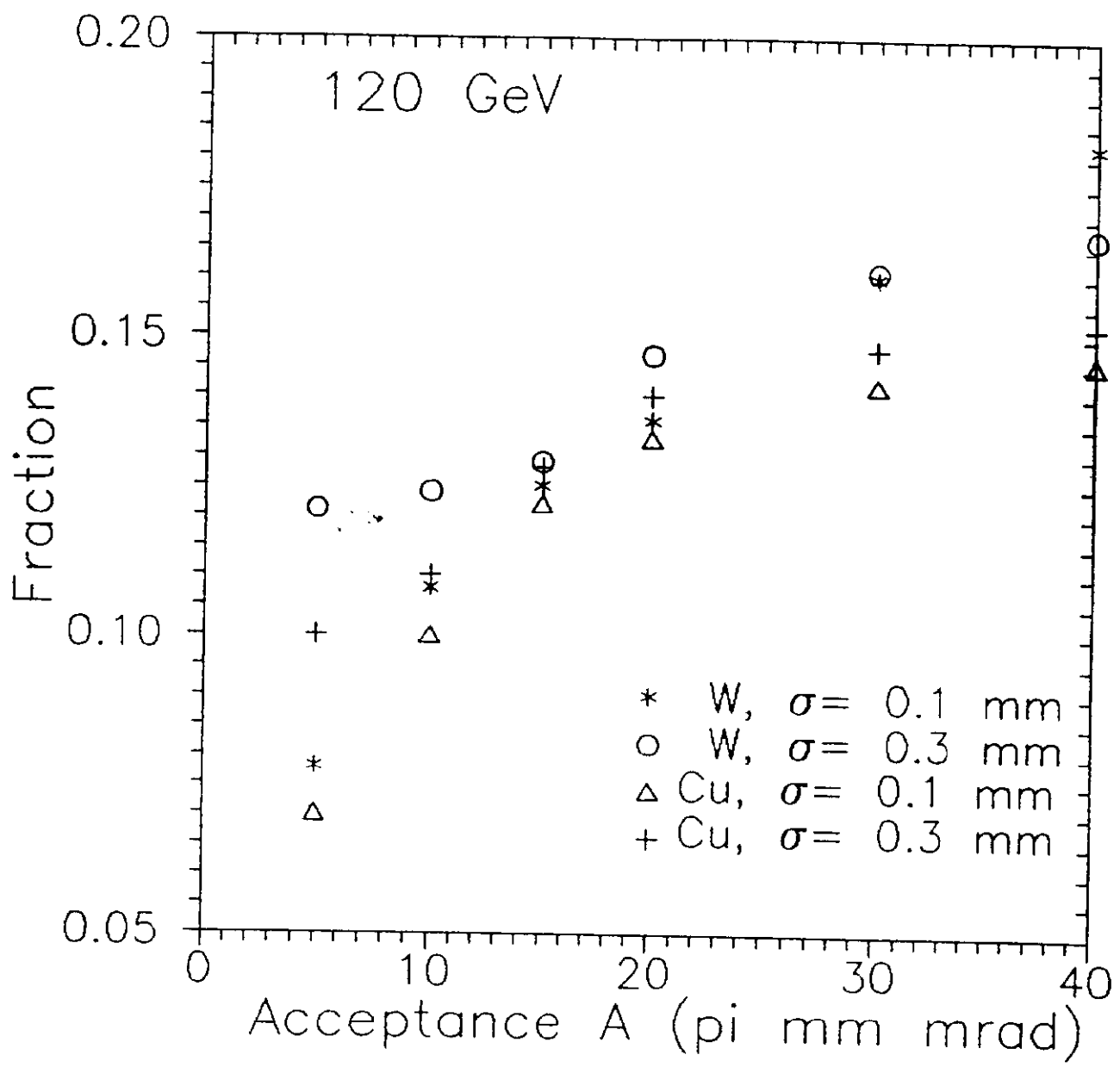
Curves - \bar{p} MARS1M

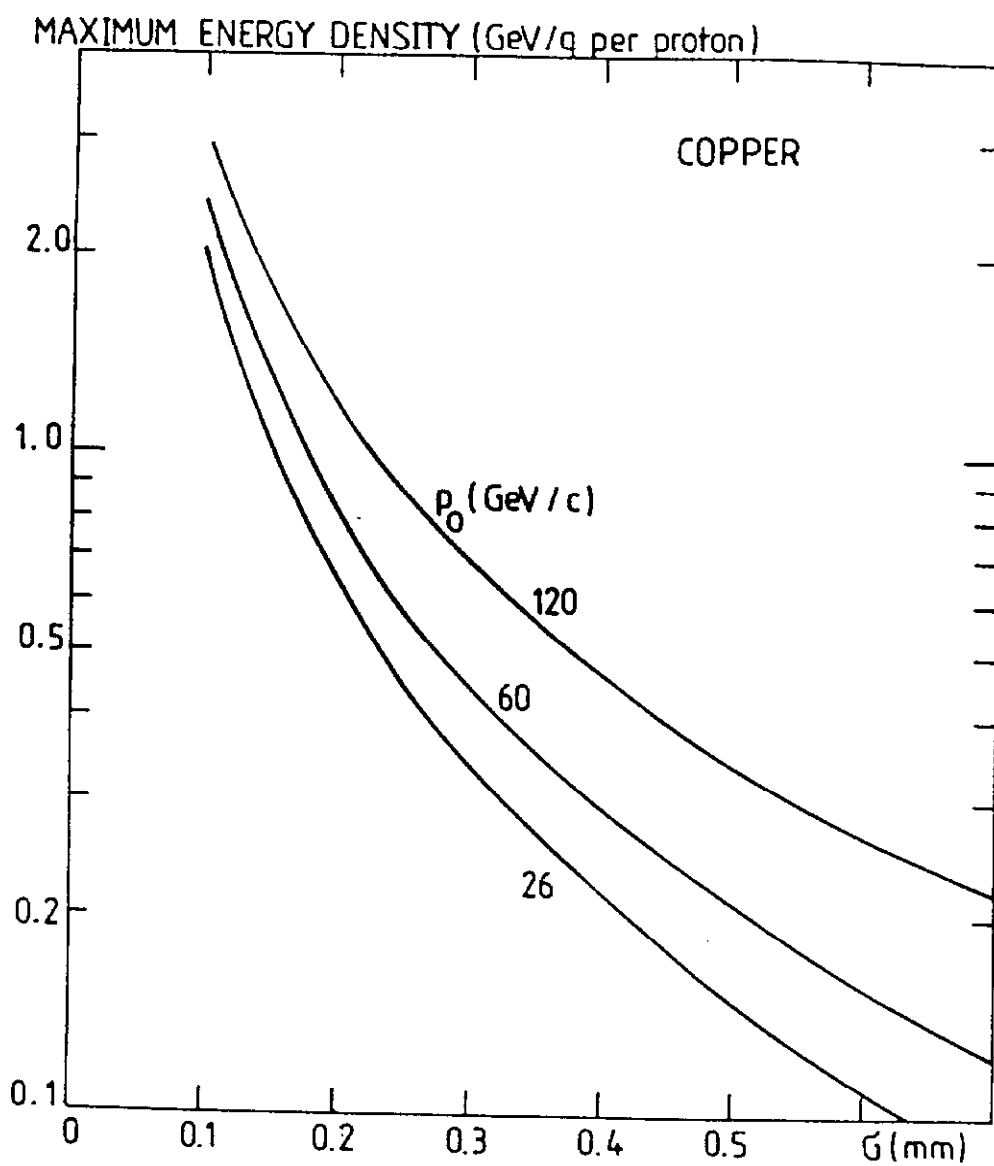


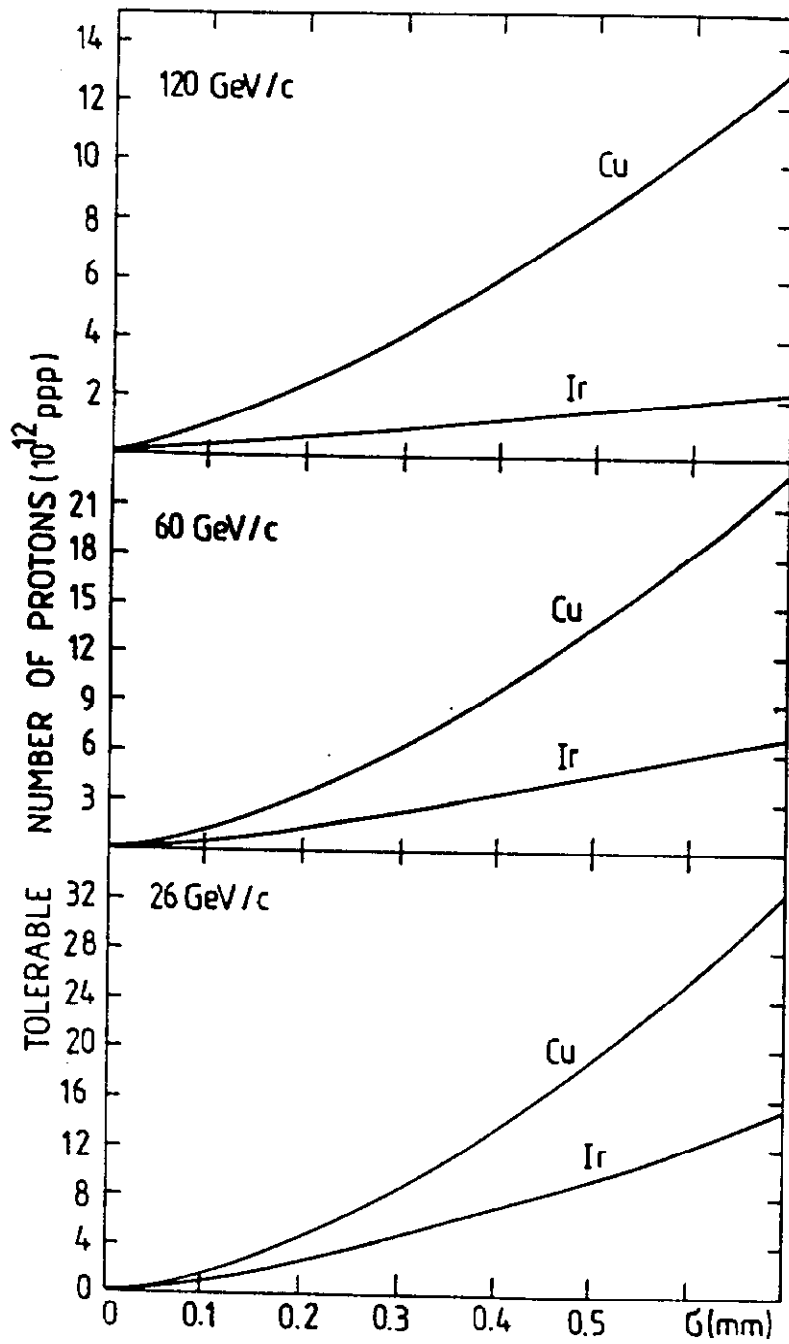


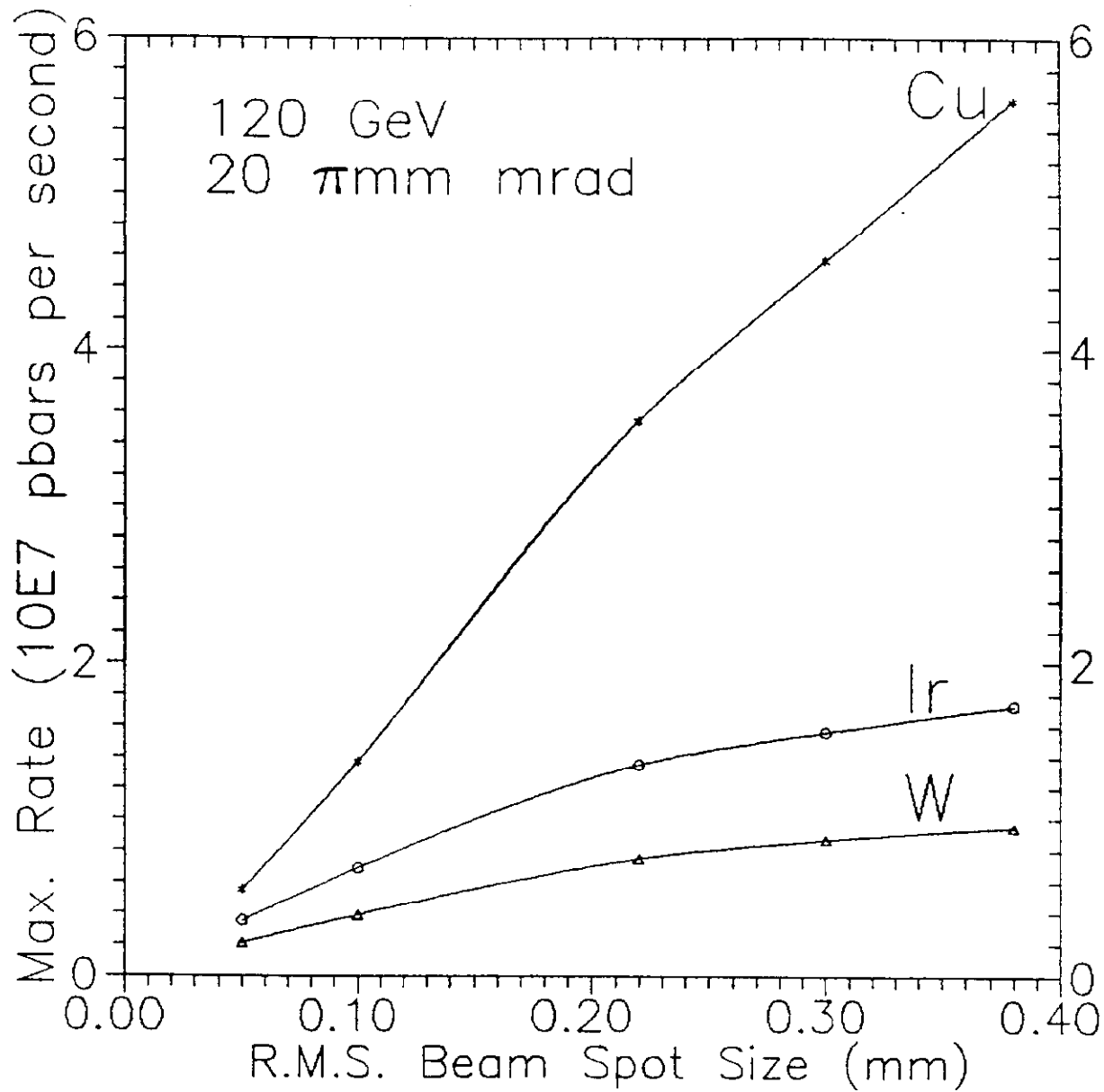


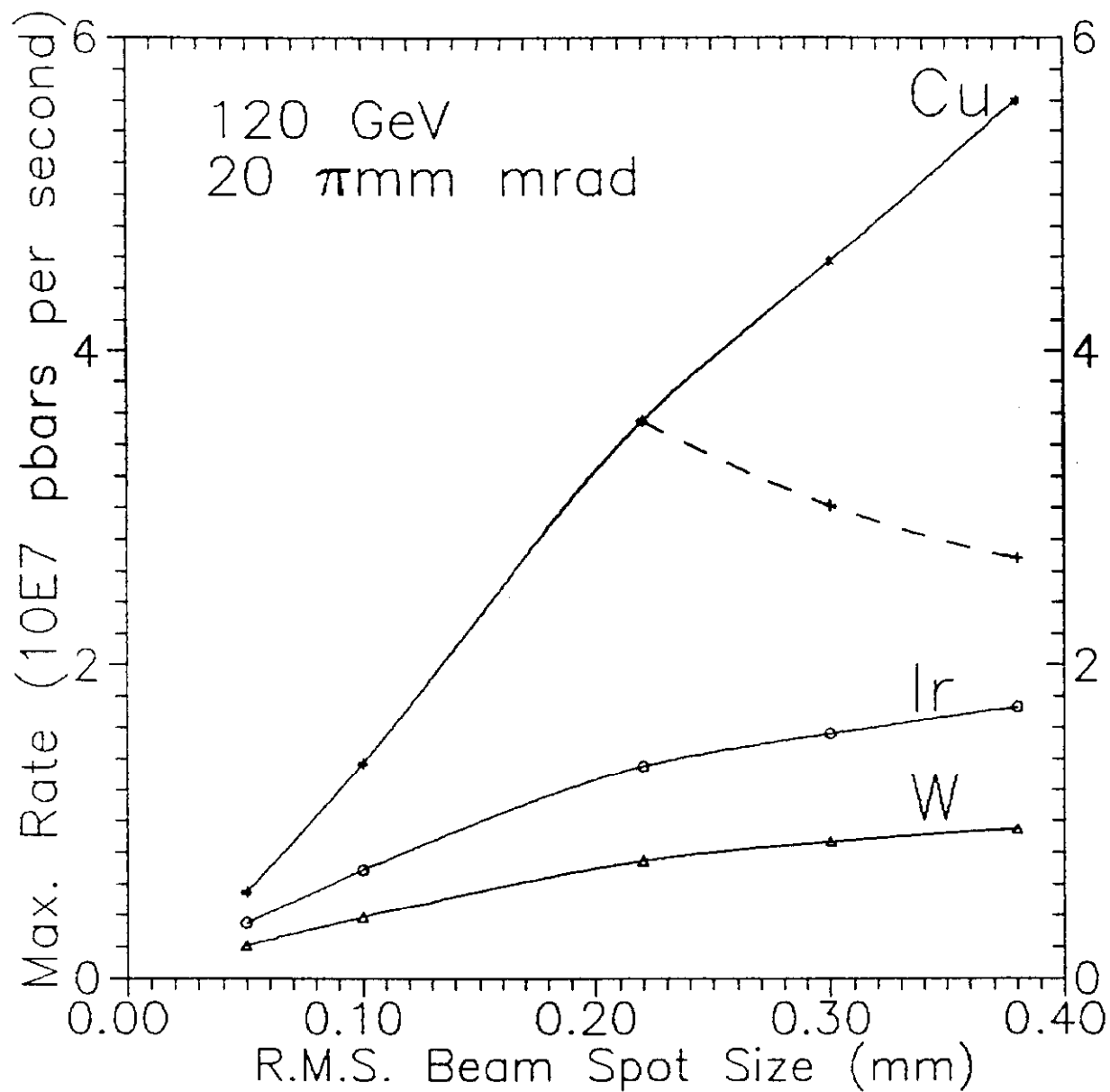












$$--- N_p^{max} \approx 3 \cdot 10^{12} \text{ ppp}$$